Remote Sensing of Environment 186 (2016) 275–285

Contents lists available at ScienceDirect

Remote Sensing of Environment

journal homepage: www.elsevier.com/locate/rse

Detecting unburned areas within wildfire perimeters using Landsat and ancillary data across the northwestern United States

Arjan J.H. Meddens [a,*], Crystal A. Kolden [a], James A. Lutz [b]

[a] College of Natural Resources, University of Idaho, Moscow, ID 83844-1133, USA
[b] Wildland Resources, Utah State University, Logan, UT 84322-5230, USA

ARTICLE INFO

Article history:
Received 26 April 2016
Received in revised form 29 June 2016
Accepted 11 August 2016
Available online xxxx

Keywords:
Landsat
Wildfire
Fire refugia
Unburned areas
Unburned islands
Fire severity

ABSTRACT

Wildfires shape the distribution and structure of vegetation across the inland northwestern United States. However, fire activity is expected to increase given the current rate of climate change, with uncertain outcomes. A fire impact that has not been widely addressed is the development of unburned islands; areas within the fire perimeter that do not burn. These areas function as critical ecological refugia for biota during or following wildfires, but they have been largely ignored in methodological studies of remote sensing assessing fire severity under the assumption that they will be detected by algorithms for delineating fire perimeters. Our objective was to develop a model for classifying unburned areas within wildfire perimeters using moderate resolution satellite (i.e., Landsat) and ancillary data. We performed field observations at locations that were unburned or lightly burned within the perimeters of 12 wildfires that burned in 2012 and 2014, and augmented this with field data previously acquired on another seven wildfires across the study region. We used randomForest and classification trees to separate burned from unburned locations with high overall classification accuracy (91.7% and 89.2%, for randomForest and classification tree methods respectively). Classification accuracy was significantly higher than the semi-automated classification products from the Monitoring Trends in Burn Severity (MTBS) program. After application of the most parsimonious and accurate classification tree model, we found that the average unburned proportion of the fires was 20% with high variability between fires (standard deviation: 16.4%). The total area of unburned islands in non-forested areas was significantly higher than the total unburned area in forested areas. Accurate detection and delineation of unburned areas is increasingly critical, as some of these unburned areas contain habitat (i.e., wildfire refugia) that are crucial for maintaining biodiversity and functioning of ecosystems, particularly given observed and projected anthropogenic climate change.

1. Introduction

Wildfires are one of the primary ecological change agents across the forests and rangelands of the inland Pacific Northwest (Agee, 1993). Climate change is projected to cause increases in wildfire activity in this region (Littell et al., 2010; Spracklen et al., 2009), with altered fire regimes likely to affect availability of ecosystem services, habitat connectivity, and forest regrowth. For example, in 2014 Washington State experienced its largest wildfire in recorded history (i.e., the 104,000 ha Carlton Complex), a record that was subsequently broken in 2015 by the even larger Okanogan Complex fires (123,000 ha). Wildfires generally support increased diversity of forest structure across the landscape, i.e., different successional stages (Kane et al., 2013; Swanson et al., 2010) and biodiversity (Noss et al., 2006; Roberts et al., 2008), by burning in a heterogeneous pattern of intensity and severity across the landscape. However, there is concern that climate change may reduce such heterogeneity, with negative ecological impacts (Kolden et al., 2015a; Savage et al., 2013). Similarly, fire exclusion and other anthropogenic influences can alter fire regimes and burn severity (Becker and Lutz, in press) leading to ecosystems with reduced ecological functioning and increased vulnerability to future disturbances (Smith et al., 2014; Smith et al., 2016). Given the potential for external drivers to fundamentally alter fire regimes and ecosystem vulnerability, there is a critical need to identify metrics of fire resilience ("fire normals") that can be quantified and monitored objectively over time (Lutz et al., 2011; van Wagtendonk and Lutz, 2007).

There has been considerable literature published in the last two decades on detection of burn severity and fire effects from remote sensing. These studies have focused on identifying spectral sensitivity to fire effects, with some of the more recent work (e.g., Cansler and McKenzie, 2012; Kolden and Rogan, 2013) exploring novel approaches and the application of indices developed from earlier work to new biomes. Somewhat consistently, however, the vast majority of these studies have focused on classification of burned pixels within a fire perimeter. What remains unresolved is the sensitivity of indices at the interface

* Corresponding author.
E-mail address: ameddens@uidaho.edu (A.J.H. Meddens).

http://dx.doi.org/10.1016/j.rse.2016.08.023
0034-4257/

between completely unburned locations within the fire, and just barely burned locations within the fire (i.e., very low severity) such that this distinction could be made spectrally. Kolden et al. (2012) highlight the challenges of spectrally discriminating the unburned forest from the lightly burned; these include canopy obstruction of fire effects in the sub-canopy, spectral mixing within pixels, illumination angle differences and/or phenological mismatch between pre- and post-fire scenes that obscures fire effects, and vegetation regeneration obscuring fire effects.

Landscape heterogeneity is important for ecosystem resilience (Peterson, 2002). Fire creates landscape mosaics influencing the landscape heterogeneity and thereby also the distribution of subsequent fires (Parks et al., 2015; Thompson et al., 2007). One potential metric of landscape resilience that has been suggested, but not widely addressed, is the unburned area where pre-fire conditions remain unchanged within a wildfire perimeter. Unburned islands that are associated with critical habitat where biota can persist (e.g., old growth forest patches) and/or provide seed sources for adjacent burned areas are defined as wildfire refugia (Camp et al., 1997; Swengel and Swengel, 2007). These areas also provide shelter for a range of fauna post-fire and can reduce detrimental impacts on hydrology and erosion, however, increased burn severity due to anomalously hot and dry weather can lead to a decrease in unburned areas within the fire perimeter (Kane et al., 2015a; Kolden et al., 2015a). Therefore, accurate detection of unburned islands is important, both for natural resource management focused on maintaining or promoting wildfire refugia on the landscape and for ecological research that seeks to understand wildfire impacts. Although low-intensity fires can maintain fire-resistant vegetation and support fire refugia in addition to unburned islands, mapping of unburned islands is a conservative approach to identifying fire refugia.

Moderate resolution satellite sensors, such as the Landsat Thematic Mapper (TM) and its successors, have been employed for detecting ecological disturbances and monitoring wildfire impacts since 1982 (e.g., White et al., 1996). Progress in remote sensing of wildfire extent and effects includes development of the Normalized Burn Ratio (NBR), a spectral index that is calculated from near infrared and shortwave infrared bands and is sensitive to decreases in photosynthetically active vegetation, increases in mineral soil, and decreases in soil moisture (i.e., proportional to the degree of environmental change caused by the fire; Key and Benson, 2006). Although the NBR has been criticized as sub-optimal index for assessing burn severity (Roy et al., 2006), the NBR and the difference between pre-fire and post-fire NBR (dNBR; Key and Benson, 2006) are widely used for detection of effects of wildland fires and other disturbances across the US and elsewhere (e.g., De Santis and Chuvieco, 2007; Sparks et al., 2015). More recently, a relativized dNBR index (RdNBR) has been proposed by Miller and Thode (2007), that adjusts dNBR for the level of pre-fire vegetation, and has improved burn severity estimation in California and the southwestern United States (Miller et al., 2009a), although not necessarily across all forest types in the US (Cansler and McKenzie, 2012). These indices have been correlated to various field measures of fire effects, including both specific forest biometrics (e.g., Miller et al., 2009a) and composite measures at equivalent spatial extents (e.g., Key and Benson, 2006). They have also been assessed for accuracy in identifying the perimeter of wildfire burned area (Kolden and Weisberg, 2007; Sparks et al., 2015), but not yet for delineating unburned areas within the fire.

The Monitoring Trends in Burn Severity (MTBS) project (http://www.mtbs.gov/; accessed March 2nd 2016) creates burn severity maps for fires ≥405 ha (1000 acres) in the western United States and ≥202 ha (500 acres) in the eastern United States using Landsat TM data from 1984 to the present using a semi-automated image analysis approach (Eidenshink et al., 2007). MTBS data includes thematic burn severity maps with categories of unburned, low severity, moderate severity, high severity, and advanced greenness, however, the classification thresholds are determined subjectively in an inconsistent manner (Kolden et al., 2015b). Because MTBS is arguably the most widely used burn severity data set (e.g., Hicke et al., 2013), identifying algorithmic improvements in severity threshold determination could have broad applicability.

Most recent research in satellite-detected burn severity has focused on higher severity fire (e.g., Dillon et al., 2011; Lutz et al., 2009; Miller et al., 2009b), while the lower end of the burn severity spectrum has largely been understudied (Kolden et al., 2012). The unburned area, and hence the ecological resilience within fire perimeters, can be substantial. Abatzoglou and Kolden (2013) and Kolden et al. (2012, 2015a) found that delineation of unburned area from MTBS averaged between 20% and 25% across ecoregions of the western United States. These analyses relied on classified dNBR severity data using two different methods, both of which were highly subjective. Kolden et al. (2012, 2015a) used the arbitrary thresholds recommended by Key and Benson (2006), while Abatzoglou and Kolden (2013) used the unburned class derived from the semi-automated and subjective classification method employed by MTBS. To-date, there has been no quantitative analysis identifying the most accurate method for delineation of unburned islands from spectral data.

Our objectives in this study were to 1) accurately classify unburned islands within fire perimeters, 2) quantify the increase in accuracy over methods utilized in prior efforts focused more broadly on burn severity (i.e., MTBS), and 3) quantify the unburned proportion of the analyzed wildfires. We sampled unburned-to-low severity field sites within 12 recent fires throughout the inland Pacific Northwest of the US and used plot data from previous studies of seven additional fires. We investigated two non-parametric methods (Classification and Regression Trees; Breiman et al., 1984 and Random Forests; Breiman, 2001) to delineate burned from unburned areas, using both Landsat-derived and topographic variables as potential predictors of unburned islands. We then applied our most accurate model to delineate unburned islands across all fires, and compared our classification to the subjective thematic maps produced by MTBS.

2. Methods

2.1. Study area

The study area covers the inland Pacific Northwest (Washington, Oregon, and Idaho), and includes 19 large fires that burned from 2006 to 2014 (Fig. 1). We sampled within 12 fires that burned in 2012 and 2014 (Table 1) and also acquired existing field data from prior studies of seven other fires that used equivalent protocols (Table 2) to increase both the number of plots and the range of burning conditions, as both 2012 and 2014 were regional fire years and represent climatic anomalies. Within the study area, vegetation varies from shrub and grassland communities at lower elevations to mixed-conifer forests at middle elevations to subalpine fir and Engelmann spruce forests at higher elevations (Franklin and Dyrness, 1988). The topography ranges from high elevation mountains of the Cascades to large, relatively topographically flat basins and rolling hills east of the Cascades that eventually meet the mountainous areas of the Northern Rocky Mountains to the east (Fig. 1). The climate in the inland Pacific Northwest ranges from semi-arid steppe in the Columbia (WA) and Harney (OR) Basins to more mesic and cooler conditions in the Cascades Mountains along the western perimeter and the Rocky Mountains along the eastern edge.

2.2. Field data collection

In 2013 and 2015, we collected field data from 12 fires that burned in 2012 and 2014. Fires were selected to span a range of vegetation types including grasslands and shrublands as well as early seral and mature closed canopy forest. Additional selection criteria included accessibility (sampling occurred primarily on state and federal ownership lands) and availability of cloud-free Landsat pre-fire and post-fire scenes. To

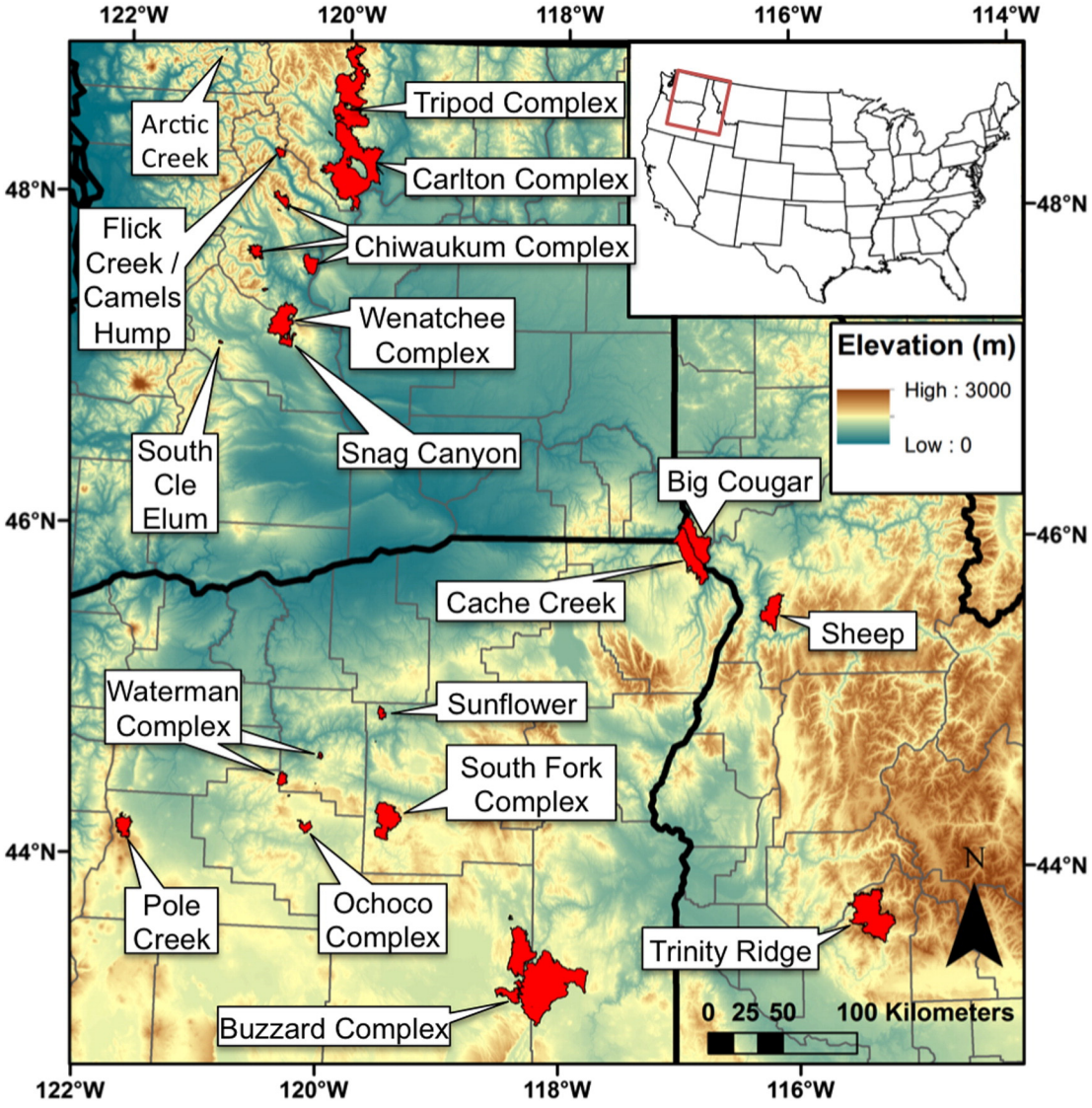

Fig. 1. Sampled fires in this study (the inset shows the location of the map in the United States).

minimize effects from edges, roads, and spatial autocorrelation, we generated randomly located field sampling locations that satisfied the following constraints: 1) >100 m from any other sampling location, 2) >100 m inside the fire perimeter, 3) >50 m from any road, and 4) located in areas that appeared to be unburned by visually inspecting pre-fire and post-fire Landsat scenes. We loaded all candidate locations into a

Table 1
Summary of fire names, fire start dates, field plot numbers, and Landsat scenes used to detect unburned areas for plot data that was purposely collected for this study and placed in low or unburned areas.

Fire name (state)	Abrev.	Area (ha)	Year	Start fire date	No. of plots		Path/row	Sensor (image acquisition day of year and year)			
					Burned	Un-burned		Pre-fire image (immediate)	Post-fire image (immediate)	Pre-fire image (1-year)	Post-fire image (1-year)
Buzzard complex (OR)	BUZ	160,153	2014	14 Jul	2	7	43/30	TM8(243-2013)	TM8(246-2014)	TM8(182-2014)	TM8(201-2015)
Big Cougar Fire (ID)	BCF	26,385	2014	2 Aug	6	4	42/28	TM8(204-2013)	TM8(239-2014)	TM8(191-2014)	TM8(210-2015)
Ochoco Complex (OR)	OCH	5067	2014	13 Jul	18	12	44/29	TM8(243-2013)	TM8(253-2014)	TM8(157-2014)	TM8(176-2015)
South Fork Complex (OR)	SFC	26,782	2014	1 Aug	13	9	44/29	TM8(250-2013)	TM8(253-2014)	TM8(157-2014)	TM8(176-2015)
Sunflower (OR)	SUN	2904	2014	14 Jul	30	0	44/29	TM8(250-2013)	TM8(253-2014)	TM8(157-2014)	TM8(176-2015)
Waterman Complex (OR)	WAT	5067	2014	11 Jul	47	2	44/29	TM8(250-2013)	TM8(253-2014)	TM8(157-2014)	TM8(176-2015)
Carlton Complex (WA)	CAR	103,643	2014	14 Jul	103	2	45/26	ETM+(201-2013)	TM8(244-2014)	TM8(196-2014)	TM8(183-2015)
Snag Canyon (WA)	SNC	12,599	2014	2 Aug	17	4	45/27	TM8(225-2013)	TM8(244-2014)	TM8(196-2014)	TM8(183-2015)
Chiwaukum Complex (WA)	CHI	5099	2014	15 Jul	37	3	45/27	TM8(225-2013)	TM8(244-2014)	TM8(196-2014)	TM8(183-2015)
Sheep (ID)	SHP	19,678	2012	6 Sept	15	12	42/28	TM5(247-2011)	ETM+(274-2012)	TM5(215-2011)	TM8(156-2013)
Cache Creek (OR)	CCHCR	29,824	2012	20 Aug	18	36	42/28	TM5(247-2011)	ETM+(274-2012)	TM5(215-2011)	TM8(156-2013)
Trinity Ridge Complex (ID)	TRNY	59,421	2012	3 Aug	3	30	41/30	TM5(272-2011)	ETM+(251-2012)	TM5(224-2011)	TM8(181-2013)

Table 2
Summary of fire names, fire start dates, field plot numbers, and Landsat scenes used to detect unburned areas for plot data collected not purposely for this study and spanning a broader burn severity range than the fires listed in Table 1.

Fire name (state)	Abrev.	Area (ha)	Year	Start fire date	No. of plots		Path/row	Sensor (image acquisition day of year and year)			
					Burned	Un-burned		Pre-fire image (immediate)	Post-fire image (immediate)	Pre-fire image (1-year)	Post-fire image (1-year)
South Cle Elum Ridge (WA)	CLE	362	2014	7 Aug	36	0	45/27	TM8(225-2013)	TM8(244-2014)	TM8(196-2014)	TM8(183-2015)
Pole Creek (OR)	PC	10,844	2012	9 Sept	68	5	45/29	TM5(300-2011)	ETM+(279-2012)	TM5(188-2011)	TM8(161-1013)
Wenatchee Complex (WA)	WCF	22,780	2012	9 Sept	115	7	45/27	TM5(252-2011)	ETM+(279-2012)	TM5(236-2011)	TM8(161-2013)
Camel Humps (WA)	CAMH	53	2008	Jul	23	5	46/26	TM5(245-2007)	TM5(251-2008)	TM5(248-2007)	TM5(253-2009
Artic Creek (WA)	ARCR	35	2008	Jul	19	5	46/26	TM5(245-2007)	TM(251-2008)	TM5(248-2007)	TM5(253-2009
Flick Creek (WA)	FLCR	2856	2006	26 Jul	99	0	45/26	TM5(219-2005)	TM5(270-2006)	TM5(219-2005)	TM5(209-2007)
Tripod (WA)	TRIP	70,753	2006	24 Jul	53	3	45/26	TM5(219-2005)	TM5(270-2006)	TM5(219-2005)	TM5(209-2007)

handheld GPS and field crews navigated to as many as these plots as was possible given constraints of safety, accessibility, and time. Once field crews had navigated to each candidate location, they assessed whether the plot (30 m × 30 m) was located in an area of relatively homogenous vegetation and burn severity category. If not, they moved the minimum distance required to relocate the plot center such that the plot would meet the criteria of Key and Benson (2006), i.e., representing the range of variability found at the site and falling within a larger homogeneous area of the same burn severity.

Plots were established following the Composite Burn Index (CBI) protocol described in Key and Benson (2006). The CBI is an aggregate measure of fire effects that is specifically meant to calibrate Landsat spectral indices; it is a composite score ranging from 0 to 3 of several ocularly-estimated fire effects ratings for different strata of the vegetation in the plot, where zero is equivalent to unburned and three is the maximum fire-induced change (Key and Benson, 2006). In addition to the CBI protocol, we collected vegetation structure and species information at each plot. The plot location was collected by a Garmin WAAS-enabled (Wide Area Augmentation System) GPS (Model Etrex 30) for at least 15 min at the center of each plot.

Although we were targeting unburned areas for plot establishment through pre-field stratification of plots by visual assessment of Landsat data, we ultimately collected field data in 121 plots that were unburned and 309 plots that were somewhat affected by fire. Due to time constraints and accessibility issues, some larger fires had lower plot numbers than targeted (e.g., the Buzzard Complex). To increase the number of truly unburned plots, we used field data from 438 plots from seven other recent fires (i.e., Bleeker, 2015; Cansler and McKenzie, 2012; Table 2). This resulted in 868 plots across 19 wildfires (Tables 1 and 2). We reclassified the plots into unburned (plots with a CBI score equal to 0) and burned plots (plots with a CBI score > 0) for further analysis (Fig. 2).

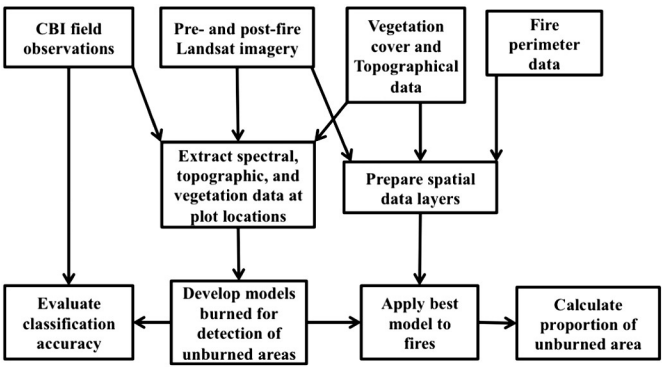

Fig. 2. Workflow indicating the actions performed in this study. CBI: Composite Burn Index.

2.3. Landsat, topographic, and vegetation data

We obtained Climate Data Record (CDR) Landsat scenes that were processed to surface reflectance from the USGS EarthExplorer (http://earthexplorer.usgs.gov, accessed 29 September 2015) (Fig. 2). All CDR scenes were Level 1T (L1T) terrain-corrected Landsat data that were atmospherically corrected by the Landsat Ecosystem Disturbance Adaptive Processing System (LEDAPS; Masek et al., 2006). In addition to the processing of the data to at-surface reflectance, CDR scenes include an automatically generated cloud and cloud shadow mask (CFmask; Zhu and Woodcock, 2012) that was used to mask image portions that contained clouds and cloud shadows that obscured the Earth's surface in the imagery.

We obtained two scene pairs for each fire (Tables 1 and 2). The first scene pair was acquired approximately one-year before the fire (pre-fire) and within the same year as the fire (post-fire) as close to anniversary dates as possible, and is referred to as *immediate post-fire* (Fig. 3). The second image pair was acquired during the same growing season (usually July or August) as the fire (pre-fire) and approximately one year following the fire (post-fire) as close to anniversary dates as possible, and is referred to as *1-year post-fire* (Fig. 3). Both image timing periods are generally used in post-fire ecosystem analyses, although the Burned Area Emergency Response (BAER) (http://www.fs.fed.us/biology/watershed/burnareas/index.html; accessed March 2nd 2016) program generally uses the immediate post-fire imagery pair for immediate post-fire effects assessments and soil erosion prevention, whereas the MTBS program generally uses 1-year post fire imagery to be able to capture the a more complete range of effects of the fire, as tree mortality often occurs in the months following a wildfire (Eidenshink et al., 2007; Key, 2006).

To separate the unburned from the burned pixel locations, we transformed the Landsat reflectance to several indices that have been shown to be sensitive to vegetation and ecological disturbances (Table 3). These indices include the Normalized Burn Ratio (NBR; Key and Benson, 2006), Normalized Differenced Vegetation Index (NDVI; Tucker, 1979), the Band 5/Band 4 ratio (B5B4; Vogelmann, 1990; Vogelmann and Rock, 1988), the Normalized Differenced Moisture Index (NDMI; Wilson and Sader, 2002), and the Tasseled Cap Brightness (TCBRI), Wetness (TCWET), and Greenness (TCGRE) (Crist, 1985; see Table 3 for formulae). Because the Landsat band numbers changed with Landsat Operational Land Imager (OLI), we used the appropriate bands equivalent to the wavelength centers associated with TM (i.e., B5B4 was calculated using Band 6 and Band 5 from OLI), and hereafter use TM band naming conventions for continuity. In addition to the post-fire indices, we also calculated differenced indices to represent changes from pre- to post-fire. As differenced images include vegetation that is often in different phenological stages in the two temporal windows in addition to any wildfire impacts, we corrected for phenological differences for each index by subtracting the mode of the differenced values of the undisturbed natural vegetation (i.e., excluding agricultural and urban areas) outside of the fire perimeter following Key

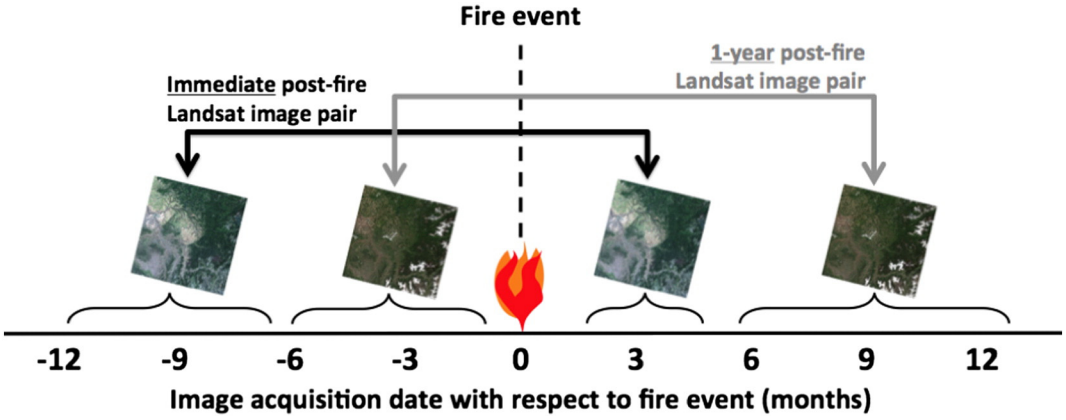

Fig. 3. Illustration of the timing of image acquisition date with respect to the fire event, modified from Key and Benson (2006). Both the immediate and 1-year post-fire Landsat image pairs were used in this study.

(2006). For example, the corrected, differenced NBR ($dNBR_{corr}$) was calculated as follows:

$$dNBR_{corr} = (NBR_{prefire} - NBR_{postfire}) - Mode(NBR_{prefire} - NBR_{postfire}) \quad (1)$$

where $Mode(NBR_{prefire} - NBR_{postfire})$ is the mode (or histogram peak) value of the differenced NBR surrounding the fire perimeter (Fig. S1). We clipped all data layers to a rectangular window of approximately 500 pixels (or 15 km) in all directions away from the furthest fire perimeter extent in each cardinal direction to calculate the undisturbed mode of the differenced NBR value. The phenological correction improved the relationship between dNBR and field measured burn severity over uncorrected dNBR (Fig. S2). All subsequent analyses utilizing differenced indices were conducted with phenologically-corrected data, including the Relative differenced. Normalized Burn Ratio (RdNBR; Miller and Thode, 2007, Table 2).

Because both vegetation type and topography are related to burn severity across the landscape (e.g., Dillon et al., 2011; Hammill and Bradstock, 2006), these characteristics might be important for locating unburned areas as well. Therefore, we obtained topographic and vegetation data from the LANDFIRE program (Rollins, 2009) that was available for the entire the study area. Topographic data included elevation, slope, and aspect. Vegetation data included the LANDFIRE Existing Vegetation Type (EVT) product for 2012 (Version: lf 1.3.0, www.LANDFIRE.gov, accessed: 30 September 2015). We selected a limited number topographical indices that were successfully used in previous studies to calculate explanatory variables for input into a classification analysis, including slope (SLOPE), the cosine of the aspect (cosASPECT), transformed aspect (TRASP; Roberts and Cooper, 1989), southwestern aspect (SWASP; Ohmann and Spies, 1998), and an interaction coefficient of the slope and aspect (SCOSA; Stage, 1976) (Table 3). LANDFIRE EVT life form attributes were used to stratify both plots (for model development) and imagery (for prediction) into forested and non-forested classes. The non-forested class included the EVT classes of herb, shrub, water, barren, and developed, while the forested class only included the tree class.

Table 3
Predictor variables considered in the classification (bands (B) refer to TM band order).

	Index	Abbrev.	Formula	Notes	Reference
Remotely sensed indices	Normalized burn ratio	NBR	$\frac{(B4 - B7)}{(B4 + B7)}$	Sensitive to wildfire effects to ecosystems	Key and Benson, 2006
	Normalized difference vegetation index	NDVI	$\frac{(B4 - B3)}{(B4 + B3)}$	Sensitive to green (healthy) vegetation	Tucker, 1979
	Band5/Band4 ratio	B5B4	B5 / B4	Sensitive to conifer tree health	Vogelmann, 1990, Vogelmann and Rock, 1988
	Normalized difference moisture index	NDMI	$\frac{(B4 - B5)}{(B4 + B5)}$	Sensitive to canopy water content	Wilson and Sader, 2002
	Tasseled cap brightness	TCBRI	$0.2043 * B1 + 0.4158 * B2 + 0.5524 * B3 + 0.5741 * B4 + 0.3124 * B5 + 0.2303 * B7$	Sensitive to surface brightness	Crist, 1985
	Tasseled cap greenness	TCGRE	$-0.1603 * B1 - 0.2819 * B2 - 0.4934 * B3 + 0.7940 * B4 - 0.0002 * B5 - 0.1446 * B7$	Sensitive to vegetation greenness	
	Tasseled cap wetness	TCWET	$0.0315 * B1 + 0.2021 * B2 + 0.3102 * B3 + 0.1594 * B4 - 0.6806 * B5 - 0.6109 * B7$	Sensitive to vegetation vigor (water content)	
	Relative differenced normalized burn ratio	RdNBR	$\frac{(NBR_{prefire} - NBR_{postfire}}{\sqrt{NBR_{prefire}/1000}}$	Sensitive to relative changes caused by wildfires	Miller and Thode, 2007
Topographic indices	Slope	SLOPE	Slope in degrees	Steepness	-
	Cosine of Aspect	cosASPECT	cos(Aspect)	Gradient from north to south facing aspects	-
	Transformed aspect	TRASP	$1 - \cos * (PI / 180) * Aspect - 30$	Gradient from northwestern to southeastern facing aspects	Roberts and Cooper, 1989
	Southwestern aspect	SWASP	$\cos((45 - Aspect / PI)) + 1$	Gradient from northwestern to southeastern facing aspects	Ohmann and Spies, 1998
	Slope cosine aspect	SCOSA	$Slope * \cos(Aspect)$	Interaction coefficient between slope and aspect	Stage (1976)

2.4. Classification and accuracy assessment

We used two non-parametric classification techniques to delineate unburned from burned pixels: Classification and Regression Trees (CART; Breiman et al., 1984) and Random Forest (RF; Breiman, 2001). Both techniques are widely used in remote sensing studies and generally achieve high classification accuracies (e.g., Falkowski et al., 2009; Hudak et al., 2008; Lawrence and Wright, 2001). CART and RF are non-parametric and are thus unaffected by parametric statistical assumptions (i.e., normality and homoscedasticity). In addition, both techniques can handle non-linear variable interaction and both categorical and continuous explanatory variables (De'ath and Fabricius, 2000).

Our response variable was a binary variable of either burned or unburned, and the explanatory data comprised the Landsat indices for immediate post-fire (indicated with an *i*), Landsat indices one-year post fire (indicated with an *y*), the differenced indices (generated from the immediate post-fire and one-year post-fire), and the topographic variables. Even though CART and RF are less sensitive to multicollinearity (Speybroeck, 2012), we wished to exclude redundant explanatory variables from our modeling approach. Therefore, we selected only indices that have been used in detecting vegetation dynamics (Table 3) and used QR matrix decomposition (Becker et al., 1988) to test whether our explanatory variables exhibited multicollinearity (Falkowski et al., 2009). None of the explanatory variables showed multicollinearity and we thus proceeded with all 35 variables in the full model (see Table 4 for a full list). Subsequently, we ran the classifications for different combinations of explanatory variables (i.e., all variables, all variables excluding immediate post-fire imagery, all variables excluding one-year post-fire imagery, and only one year post-fire dNBR and RdNBR) to assess the predictive power of using different sets of explanatory variables related to the timing of data acquisition relative to the timing of the fire.

2.4.1. Classification trees

The CART technique is a recursive partitioning method that uses binary divisions to split the data until terminal nodes are found given preset criteria (Breiman et al., 1984). Explanatory variables are analyzed to find the most accurate split given the reduction in deviance in the response variable (Lawrence and Wright, 2001). Trees are refined until a new split does not increase the accuracy of the tree or until a predetermined number of splits is reached. CART dendrograms are easily interpretable and easy to apply to large volumes of (remote sensing) data.

Calculations were performed in R (version 3.2.3, R Core Team, 2015), using the rpart package (Version 4.1-10, Therneau et al., 2015). The rpart package was run in classification mode with an initial complexity parameter of 0.001. The parsimonious final tree was determined by pruning the preliminary tree with the 1-standard error (se) rule (De'ath and Fabricius, 2000), where the number of splits was determined at the one standard error plus the minimum cross-validated error.

We used a ten-fold cross validation to generate an independent overall accuracy estimate. The plots that were used for the evaluation were not used in the creation of the classification tree and were randomly separated into ten approximately equal groups (of ~72 plots). The classification tree was built using nine of the groups and the classification accuracy was independently determined using the group that was left out. This was repeated 10 times, so that every group had an independent accuracy assessment. The ten individual accuracy assessments were then added together to generate an overall confusion matrix and accuracy estimate for all plots. Because the classification trees for each iteration of the cross-validation were slightly different, we generated the final model from all of the plots.

2.4.2. Random Forest

The RF algorithm uses a bootstrapping approach to parse the data and then develops many classification trees (i.e., a forest of classification trees) to find the best predictor variables. The outcome is a number of votes for a given class as opposed to a rule-based classification (as in a CART). Through the bootstrapping approach, RF creates accurate and unbiased prediction results based upon votes and generally receives higher classification accuracies than classification trees (Falkowski et al., 2009).

We used the RF algorithm implemented in R (Version 4.6-12, Liaw and Wiener, 2002) in classification mode with tree size set to 1000. The RF algorithm generates an independent out-of-the-bag (OOB) error estimate through a bootstrapping technique in which the data is subsampled to calculate a model error rate and confusion matrix from a subsample (approximately one third) of the data that is not used in the model generation (Breiman, 2001). To minimize the number of explanatory variables, we calculated the model improvement ratio (MIR; Murphy et al., 2010), and reduced the explanatory variables used in the final RF model to the number of explanatory variables as indicated by the MIR analysis. We report the mean decrease of accuracy (i.e., the reduction of the percent classification accuracy if a given variable was removed from the classification) of the ten most important explanatory variables of the best models separating the burned and unburned classes.

2.5. Model application and analysis of unburned areas

Of the 868 total plots, 133 (15.3%) returned no data values from the immediate post-fire scenes, 51 (5.9%) returned no data values from the one-year post-fire scenes. Because some plots returned no data in both immediate and one-year post-fire scenes, 149 out of 868 plot locations

Table 4
Overall accuracies for the different classification strategies and explanatory variables separating unburned and burned classes. Note that the RandomForest (RF) runs are generated from the out-of-bag predicted samples (i.e., samples not taken account in the model generation) and the accuracies from the Classification trees (CART) are generated from a 10-fold cross validation. The highest overall accuracy percentages are indicated in bold.

	Method	Subset	All variables[a]	All variables excluding immediate post-fire imagery	All variables excluding one-year post-fire imagery	One-year post-fire dNBR and RdNBR only
Combined run (no separation between forest and non-forest)	RF		**91.9%**	90.8%	90.4%	88.0%
	CART		**89.2%**	87.8%	88.7%	87.0%
Split run (forest and non-forest run)	RF		**91.5%**	90.1%	90.2%	87.1%
		F[b]	**90.8%**	90.0%	90.6%	87.8%
		NF[c]	**93.2%**	90.5%	89.6%	85.5%
	CART		87.9%	88.3%	**90.1%**	85.7%
		F[b]	88.8%	88.9%	**91.6%**	85.5%
		NF[c]	86.0%	**86.9%**	**86.9%**	87.3%

[a] All variables include: aTCBRIi, dTCBRIi, aTCGREi, dTCGREi, aTCWETi, dTCWETi, aNDVIi, dNDVIi, aNBRi, dNBRi, RdNBRi, aNDWIi, dNDWIi, aB5B4i, dB5B4i, aTCBRIy, dTCBRIy, aTCGREy, dTCGREy, aTCWETy, dTCWETy, aNDVIy, dNDVIy, aNBRy, dNBRy, RdNBRy, aNDWIy, dNDWIy, aB5B4y, dB5B4y, SLOPE, cosASPECT, TRASP, SWASP, SCOSA with i indicating Landsat index derived from immediate post-fire imagery, y indicating Landsat index derived from approximately one-year post-fire imagery, d indicating differenced (pre- and post-imagery) index and a indicating the Landsat image values after the fire (not differenced).
[b] Accuracy for the Forested plots only.
[c] Accuracy for the non-forested plots only.

(17.2%) were associated with no data values in either or both temporal periods and were excluded from the relevant analysis, resulting in 719 total plots remaining. The 719 plot locations contained 498 forested plots (74 unburned and 424 burned) and 221 non-forest plots (43 unburned and 178 burned) as determined from the LANDFIRE EVT data. The no data values in the immediate post-fire imagery had several causes. First, there was often still haze and smoke obscuring the site immediately post-fire. Second, the window for capturing cloudless scenes in the autumn is short in the inland Pacific Northwest due to both the onset of snow and the shadows associated with late season image acquisition at higher latitudes; scenes are not usable after the end of the growing season. Third, because five of our fires burned in 2012, a year when Landsat 7 was the only Landsat sensor acquiring data, we were forced to use Enhanced TM + scenes that include swaths of missing data due to the 2003 failure of the scan line corrector (SLC) for the immediate post-fire imagery (Tables 1 and 2).

We conducted four different CART and four different RF model runs to test the explanatory power of the timing and different indices of the Landsat imagery and topographical variables, including: 1) all possible variables, 2) all possible variables excluding immediate post-fire imagery, 3) all possible variables excluding one-year post-fire imagery, and 4) one-year post-fire dNBR and RdNBR only. The fourth model run was to test the accuracy of a model when only dNBR and/or RdNBR are used, as these are the indices that are automatically produced by MTBS and, thus, are available to a wider potential user group without remote sensing expertise. To account for the considerable differences in life form between forests and rangeland areas, we conducted the four CART and RF runs for a combined classification run that included all plots and another stratified by forested and non-forested groups.

To compare our classification results to the MTBS-derived classification results, we obtained MTBS classified data layers (www.MTBS.gov; accessed 21 December 2015) for the available fires (CAR, CCHCR, FLCR, SHP, TRNY, TRIP; Tables 1 and 2). We combined the MTBS low, medium, and high burn severity classes into a single burned class and compared that to our field data (note that our field plots did not include any in the 'greenup' class). We calculated a confusion matrix of the plot data and the MTBS classified data (367 plots; 78 unburned and 289 burned).

We selected the most accurate model that was parsimonious and intuitive, to classify unburned areas for all fires. We used our unburned classification to calculate the proportion of unburned areas by fire size and by proportion of pre-fire forest using simple linear regression models and Spearman's rank correlations.

3. Results

3.1. Field data

Although we attempted to purposely place plots for our field visits in unburned (or areas that had low burn severity) by visually assessing (immediate) post-fire Landsat imagery, only 28.1% (121 out of 430) plots experienced no fire consumption (i.e., were unburned, Table 1). The plots from the seven additional fires included 6.1% (25 out of 438) plots that were unburned (Table 2). The total set of field validation data included 146 unburned and 692 burned plots.

3.2. Classification accuracy

The combined run while using all variables of the CART and RF algorithms returned the highest overall accuracy, 91.9% and 89.2% respectively (Table 4). The classification of burned versus unburned using the RF algorithm generated slightly higher accuracies as compared to the CART results (Table 4). When using all variables in the combined run (i.e., not split into forest and non-forest), the RF algorithm returned a 2.7% higher overall accuracy than the (cross-validated) CART algorithm (Table 5A and B). In addition to building our CART and RF models with the collected plot data, we created different models using over- and under-sampling to balance the number of unburned and burned plots to see if we could improve model accuracy and predictive power. Because the final models were similar (not shown) to the model with the plot data, we proceeded with the model using the collected plot data (i.e., we do not present the models using over- or under-sampling).

Table 5
Confusion matrices of the (A) combined randomForest model, (B) combined classification tree model, and (C) the merged burn severity classes by the Monitoring Trends in Burn Severity (MTBS) group separating unburned and burned pixel locations. Note that the randomForest out-of-bag results and the combined 10-fold cross-validated (independent evaluation) results are reported for the randomForest and classification tree methods, respectively. Comm.: commission, acc.: accuracy, omis.: omission, and prod.: producer.

A		Field observations				
Predicted	Class	Unburned	Burned	Total	Comm. error	User acc.
	Unburned	**74**	15	89	16.9%	83.1%
	Burned	43	**587**	630	6.8%	93.2%
	Total (pixels)	117	602	719		
	Omis. error	36.8%	2.5%	Overall Acc. = 91.9%		
	Prod. acc.	63.2%	97.5%			

B		Field observations				
Predicted	Class	Unburned	Burned	Total	Comm. error	User acc.
	Unburned	**66**	27	93	29.0%	71.0%
	Burned	51	**575**	626	8.1%	91.9%
	Total (pixels)	117	602	719		
	Omis. error	43.6%	4.5%	Overall Acc. = 89.2%		
	Prod. acc.	56.4%	95.5%			

C		Field observations				
MTBS	Class	Unburned	Burned	Total	Comm. error	User acc.
	Unburned	**59**	49	108	46.4%	54.6%
	Burned	19	**240**	259	7.3%	92.7%
	Total (pixels)	78	289	367		
	Omis. error	24.4%	17.0%	Overall Acc. = 81.5%		
	Prod. acc.	75.6%	83.0%			

The explanatory variables used in the final CART that generated the highest accuracy (i.e., the combined run with all explanatory variables), were dNBRy (one-year post-fire dNBR), RdNBRi (immediate post-fire RdNBR), and the aTCBRIy (one-year post-fire TCBRI) (Fig. 4a). In the first split, the burned areas separated from the remaining cases using a dNBRy threshold of ≥23. In the second split unburned areas with <166 RdNBRi are separated from the remaining pixels. Finally, unburned and burned areas were split using a 3490 aTCBRIy threshold.

For the classification tree that generated the highest accuracy (87.9%) using all variables for the separate forest and non-forest runs, the dNBRy and aNDVIy were selected for the non-forest CART (Fig. 4b). The dNBRy threshold of ≥38 separated the burned areas from the remaining pixels and the aNDVIy < 0.49 were classified as unburned and aNDVIy ≥ 0.49 were classified as burned. The forest-only CART used the dNBRy and RdNBRi (Fig. 4c), with the dNBRy threshold of ≥25 separating the burned areas from the remaining pixels and the RdNBRi < 166 indicating unburned pixels and ≥166 indicating burned pixels. The two most important explanatory variables in the combined, all variables RF run were dNBRy and RdNBRi (Fig. 5a). The non-forest RF run selected the dNBRy and dNDVIy as the most important explanatory variables (Fig. 5b), while the forest-only RF run also selected dNBRy and RdNBRi (Fig. 5c).

All-variable models using CART (89.2%) and RF (91.9%) had higher overall accuracies than the classification accuracy of MTBS (81.5%; Table 5C). The commission errors of the unburned class (i.e., pixels incorrectly classified as burned where the field observation indicated unburned) were substantially reduced in our classification algorithms compared to MTBS. The omission errors (i.e., unburned class detected as burned) of our classification algorithms of the unburned class were higher than the MTBS classifications. This might be related to the higher number of burned plots relative to unburned plots and might indicate

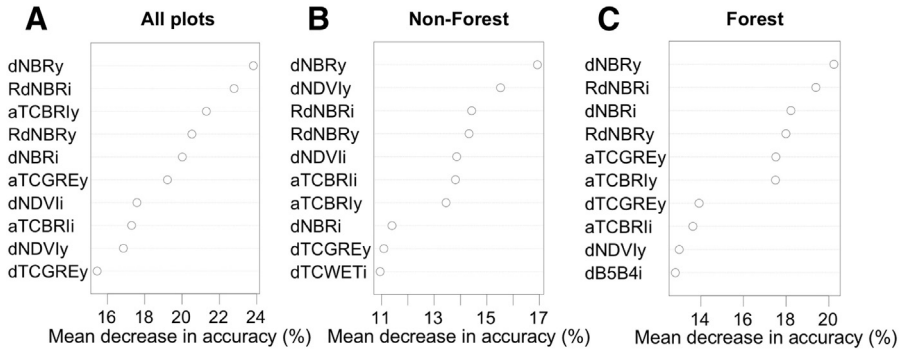

Fig. 4. Classification trees for the (a) all plots (combined), (b) non-forest, and (c) forest classifications of unburned and burned pixel locations. d: variable was differenced between a pre- and post-fire image, a: variable was taken after (post-) fire, y: one-year post-fire, i: immediate post-fire. The final nodes indicate 0: unburned, 1: burned, no. of plots classified as unburned and burned, and the percent of plots in that final node. dNBR; differenced Normalized Burn Ratio, RdNBR; Relative differenced Normalized Burn Ratio, TCBRI; tasseled cap brightness.

that our algorithms were more conservative in detecting unburned islands than the MTBS program.

3.3. Model application and spatial patterns

Although the CARTs returned slightly lower accuracies compared to the RF models, the CART models feature easily interpretable class breaks, are more parsimonious (3–4 variables, as compared to ~25 for RF), and are more efficient when applied to large datasets. The CART model derived from all variables (Fig. 4a) was applied to all fires in all years. When no data values were encountered (more prevalent in the immediate post-fire imagery), we applied the model that only used one-year post-fire imagery (Fig. S3).

The mean proportion of unburned area was 19.8% across all fires (s.d. = 16.4%). The unburned proportion was significantly greater in the non-forested areas of the fires (26.0%, standard error = 2.4) compared to the unburned proportion of the forested area of the fires (13.2%, standard error = 4.9) (two-sample *t*-test: *t*-statistic = −2.34, df = 36, p-value = 0.02). There was no significant relationship between the unburned area and fire size (Spearman's rank correlation coefficient = 0.31, p-value: 0.17; Fig. 6a) and a significant negative relationship between unburned area and the proportion of the fire that was forested (Spearman's rank correlation coefficient = −0.55, p-value: 0.01; Fig. 6b).

4. Discussion

The primary explanatory variables selected by our algorithms were variants of the NBR, but we found that using both the immediate and one-year post-fire imagery increased overall classification accuracy. While prior efforts to delineate burned from unburned area have tended to assess either immediate post-fire or one-year post-fire data, our CART

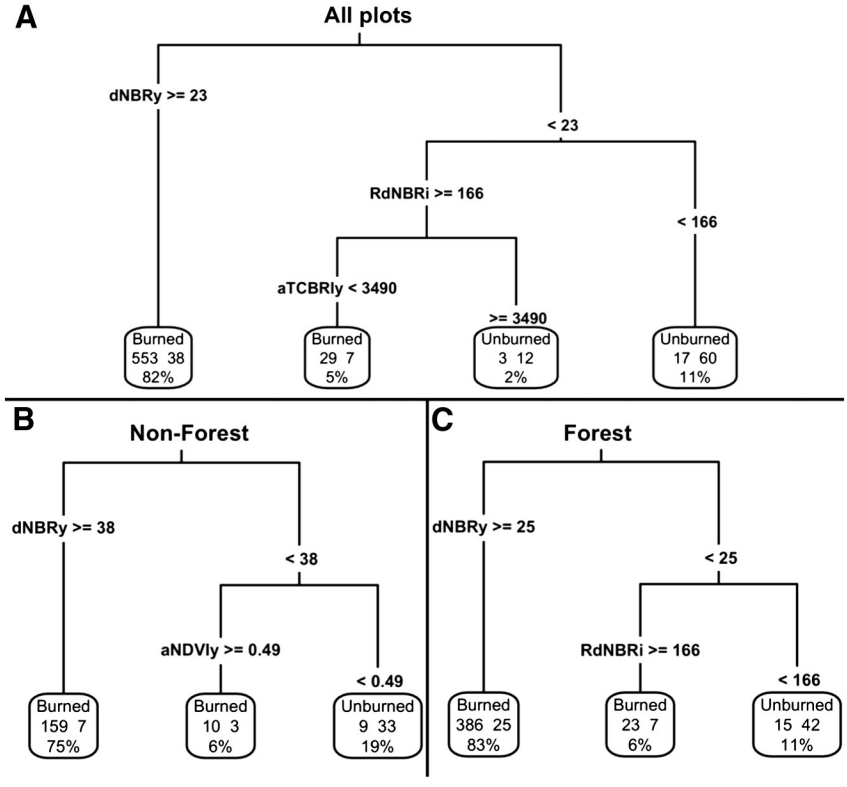

Fig. 5. Variable importance plots for (a) all plots (combined), (b) non-forest, and (c) forest randomForest classification models to separate unburned from burned pixel locations. The top 10 variables are ranked by importance from top to bottom (i.e., the exclusion of the top variable has the greatest impact on the accuracy reduction of the model). d: variable was differenced between a pre- and post- fire image, a: variable was taken after (post-) fire, y: one-year post-fire, i: immediate post-fire. The final nodes indicate no. of plots classified as unburned and burned, and the percent of plots in that final node. The variable abbreviations are given in Table 3.

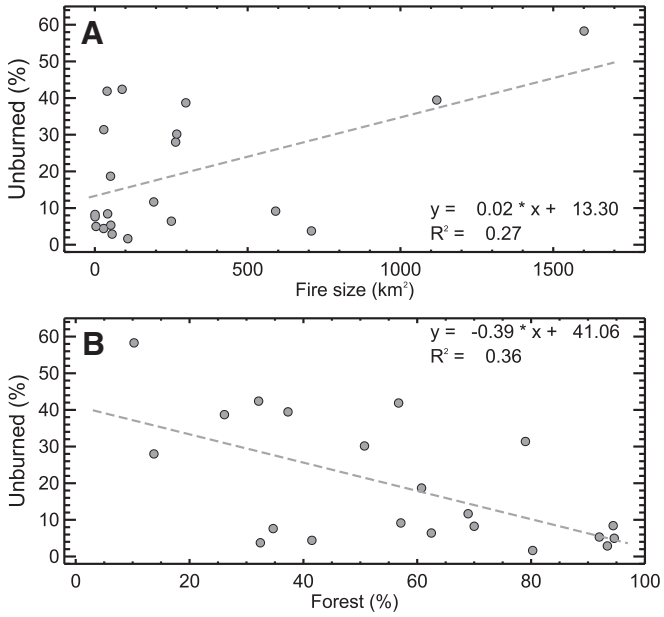

Fig. 6. (a) Unburned area versus fire size and (b) forested percentage within the fire perimeter for each fire.

and RF methods allowed for multiple years to be selected and demonstrated that a post-fire multi-temporal approach produced the highest classification accuracy. This suggests that vegetative regrowth, which is often occurring in the one-year post-fire scene, can both magnify and obscure the presence of unburned islands, and the immediate post-fire scene is needed to clarify where consumption occurred. The two non-parametric classification methods (CART and RF) generally outperformed the semi-automatic image interpretation classification performed by the MTBS program. Our methods did provide a more conservative estimate of unburned area (i.e., we produced larger omission errors compared to the MTBS classified products). This corresponds with our finding during our field campaign that some plots might visually appear unburned in the satellite imagery but might have experienced some fire effects (see Section 3.1).

Our classification of 19 inland Pacific Northwest fires resulted in nearly 20% of unburned area within fire perimeters, in agreement with previous assessments of the unburned proportion being between one-fifth and one-quarter of the area within fire perimeters (Abatzoglou and Kolden, 2013; Kolden et al., 2015a; Kolden et al., 2012). Therefore, studies using the fire perimeter to calculate an area burned overstate the magnitude of fire impacts. These unburned areas contain important habitat (Roberts et al., 2008), provide seed sources for surrounding burned areas, and contribute to overall landscape heterogeneity (Peterson, 2002; Robinson et al., 2013). Using moderate-resolution satellite remote sensing, and in particular the Landsat system, is valuable for capturing these dynamics across the landscape.

We suggest CART as the most useful classification method because its transparency (e.g., it identifies specific classification thresholds), parsimony, and efficiency when applied to large datasets, makes it more useful to managers and researchers. However, in future analyses, RF should be considered when a more accurate method is warranted. In addition, RF produces a probability rather than a hard classification, essentially calculating an uncertainty assessment (e.g., Rehfeldt et al., 2009). Our CART method produced a higher classification accuracy than MTBS, which we hypothesize is at least partially a product of using a single stationary threshold (e.g., phenologically-corrected dNBR thresholds) derived from field observations rather than per-fire image-interpreted class breaks (i.e., such as in MTBS) that lack empirical relationships with ecological effects of the fire (Kolden et al., 2015b). The combined CART separated burned pixels from others using a ≥23 dNBRy threshold; this compares to the slightly higher average threshold of ≥55 dNBR used by the MTBS in the northwestern US, although the MTBS dNBR value was not phenologically-corrected (Kolden et al., 2015b). The combined CART further separated unburned from burned areas using the RdNBRi (threshold: 166), separating areas that might have rapid revegetation one year following the fire. Finally, the aTCBRI separated burned from unburned areas, possibly separating out different spectral effects related to different vegetation types.

Our findings regarding forests versus non-forests were somewhat unexpected. We found no improvement of the classification accuracy when stratifying forested and non-forested regions. The primary reason for stratifying is the regeneration rate and "greenup" following wildfire in the two different systems; forested areas generally re-green more slowly than non-forest areas, where grasses and shrubs are often rapid resprouters in frequent fire systems. Both one-year post-fire dNBR and one-year post-fire NDVI (both the differenced and the post-fire NDVI values) were important variables for determining whether the non-forested plots were unburned or not (Figs. 4 and 5). For the forested plots, the dNBRy and RdNBRi were the two most important variables for determining whether the plots were burned or not. Once these variables were included in the model, the need to stratify plots by vegetation type was not necessary. However, our total number of non-forest plots was much smaller than the number of forest plots, and an increased sample size in non-forest areas may ultimately yield improved accuracy in classification through stratification.

There was also no clear pattern of increased or decreased detection accuracy of unburned areas within forest versus non-forest areas. Although overstory canopy can obscure low severity fire effects from passive satellite imagery (Kane et al., 2014), rapid recovery and re-greening of non-forest areas might also reduce classification accuracy. Non-forested areas, however, exhibited a greater proportion of unburned area than forested areas. This may be attributed to either less fuel continuity in non-forested areas (e.g., the BUZ fire contained very sparse vegetation cover and was ~60% unburned) as opposed to forested areas that generally have more fuel continuity, or it may be attributed to the dominant fire behavior in non-forested regions. Many of the fires in non-forested ecotypes are wind-driven fires and those fires may produce the types of rapid directions shifts and erratic fire behavior that promote creation of large unburned islands (Kolden et al., 2015a).

Phenologically-corrected spectral indices of the unburned portion of the imagery improved the consistency of application of the differenced vegetation index. The coefficient of determination of the non-linear relationship between the CBI and the one-year post-fire dNBR improved 0.03 (4.5%) when using the phenologically-corrected dNBR as opposed to the uncorrected dNBR (Fig. S2). While it has been suggested that mean values of unburned areas around the fire can be used to correct for phenology (Key, 2006), we suggest using the mode rather than the mean of the undisturbed surrounding pixels. This is because some areas (especially agricultural areas) can have significant changes in the pre- and post-fire NBR unrelated to the fire or natural vegetation phenology, possibly leading to an incorrect calculation of the phenological offset of natural areas between the two image dates.

We could not find any strong relationship between topographical variables and whether a plot was burned or not. Because there are many reasons of why an area will not burn (Kolden et al., 2012), there might not be a universal pattern (e.g., always on a north facing slope) related to topography or vegetation type that can be attributed to the chance of an area being unburned. However, patterns of burn severity likely influence probability of burning in topographical positions of certain unburned areas within given vegetation types. For instance, several recent studies found either improved accuracy in burn severity modeling when topography was included (Barrett et al., 2010; De Santis and Chuvieco, 2009; Kane et al., 2015b) or the strong influence of topography on burn severity (e.g., Birch et al., 2015; Dillon et al., 2011). Although we did not find much predictive power in topographical

variables for detecting unburned areas, further analysis of a larger and longer-term database of wall-to-wall unburned areas could reveal patterns of certain locations of unburned areas across the landscape.

We list five considerations for future research related to our study. The first consideration is the minimum size requirement to be classified as an unburned area. Landsat has a spatial resolution of 30-m, but a given pixel can include sub-pixel unburned patches. As such, unburned areas that are considerably smaller than a Landsat pixel (900 m^2) are unlikely to be detected by our algorithms. Second, the inclusion of the shortwave infrared bands on the Landsat sensor platform is important for unburned area detection as revealed by the selected explanatory variables. However, we did not test every single available index or spectral band to reduce data redundancy. An analysis of displacement within spectral space as recommended by Roy et al. (2006) and Trigg and Flasse (2001), the assessment of hyperspectral data (e.g., van Wagtendonk et al., 2004), or the inclusion of LiDAR data (Kane et al., 2014) might further improve the delineation of unburned pixels. Third, the goal of the present study was to classify unburned pixels in order that those pixels could be aggregated to map unburned patches; but uncertainty remains as to how accurately the extent and edges of larger unburned patches are delineated using this methodology. This was beyond the scope of our research and would require a validation data set that does not currently exist and would be difficult to acquire given the limitations for mapping fire edges (Kolden et al., 2012; Kolden and Weisberg, 2007). Fourth, we are unsure about the accuracy of the registration of the pixel to the plot location. Interpolation of multiple pixels adjacent to the plot location or using a plot layout designed to relate spectral data from Landsat to the field situation (e.g., Hudak et al., 2007) might further improve our results. Fifth, our approach is dependent upon readily available fire perimeters, which are currently available nationally in the US and Canada. For this model to be applied elsewhere it should be combined with automated fire perimeter delineation algorithms (e.g., Kolden and Weisberg, 2007; Sparks et al., 2015).

5. Conclusion

Unburned areas are critical for ecosystem functioning and we found that nearly 20% of the area within the fires we studied remained unburned, consistent with prior findings. We focused on spectrally delineating unburned islands within wildfires, in contrast to both earlier research focusing purely on fire perimeter edges and more recent wildfire research that has focused on quantifying and classifying higher-severity effects of fires (e.g., Cansler and McKenzie, 2012; Dillon et al., 2011; Miller et al., 2009b). We were able to detect unburned areas within different fires with a high overall classification accuracy using both RF and CARTs that primarily relied upon widely used spectral indices for assessing fire (i.e., dNBR and RdNBR) and we achieved the highest accuracy when utilizing both immediate and one-year post-fire data.

These unburned islands contain important habitat, serve as seed sources for post-fire propagation, and are ecologically important for maintaining biodiversity and ecological functioning of the ecosystems (Kolden et al., 2015a). These results will facilitate the development of a consistent historical unburned islands database for the region, yielding a wide array of applications and analyses of landscape patch dynamics, seed source evaluation, late-successional fire refugia mapping, and ecosystem resilience. Similar approaches should be undertaken for any ecoregion where a similar database is desired to investigate changes in and characteristics of unburned islands as a metric of wildfire resilience.

Acknowledgements

We thank Tyler Bleeker, Alina Cansler, and Susan Prichard for sharing valuable field data and our field crews Brian Moe, Emily Noyd, Jamie Peeler, and Martin Holdrege for their hard work. Four anonymous reviewers provided helpful comments that improved the manuscript. Funding for this work was provided by the USFS Western Wildlands Environmental Threat Assessment Center under Joint Venture Agreement 13-JV-11261900-072, NSF under award EPS-0814387, and the Department of the Interior Northwest Climate Science Center (NW CSC) through a Cooperative Agreement G14AP00177 from the United States Geological Survey (USGS). Its contents are solely the responsibility of the authors and do not necessarily represent the views of the NW CSC or the USGS. This manuscript is submitted for publication with the understanding that the United States Government is authorized to reproduce and distribute reprints for Governmental purposes.

Appendix A. Supplementary data

Supplementary data to this article can be found online at http://dx.doi.org/10.1016/j.rse.2016.08.023.

References

Abatzoglou, J.T., Kolden, C.A., 2013. Relationships between climate and macroscale area burned in the western United States. Int. J. Wildland Fire 22, 1003–1020.
Agee, J.K., 1993. Fire Ecology of Pacific Northwest Forests. Island Press, Washington, DC.
Barrett, K., Kasischke, E., McGuire, A., Turetsky, M., Kane, E., 2010. Modeling fire severity in black spruce stands in the Alaskan boreal forest using spectral and non-spectral geospatial data. Remote Sens. Environ. 114, 1494–1503.
Becker, K.M.L., Lutz, J.A., 2016. Can low-severity fire reverse overstory compositional change in montane forests of the Sierra Nevada, USA? Ecosphere (in press).
Becker, R.A., Chambers, J.M., Wilks, A.R., 1988. The New S Language: A Programming Environment for Data Analysis and Graphics. Pacific Grove, Wadsworth and Brooks/Cole.
Birch, D.S., Morgan, P., Kolden, C.A., Abatzoglou, J.T., Dillon, G.K., Hudak, A.T., Smith, A., 2015. Vegetation, topography and daily weather influenced burn severity in central Idaho and western Montana forests. Ecosphere 6, 1–23.
Bleeker, T.M., 2015. Sustainability of Historical Wildfire Refugia in Contemporary Fire Events. University of Idaho Thesis, Moscow, ID.
Breiman, L., 2001. Random forests. Mach. Learn. 45, 5–32.
Breiman, L., Friedman, J., Stone, C.J., Olshen, R.A., 1984. Classification and Regression Trees. CRC press.
Camp, A., Oliver, C., Hessburg, P., Everett, R., 1997. Predicting late-successional fire refugia pre-dating European settlement in the Wenatchee Mountains. For. Ecol. Manag. 95, 63–77.
Cansler, C.A., McKenzie, D., 2012. How robust are burn severity indices when applied in a new region? Evaluation of alternate field-based and remote-sensing methods. Remote Sens. 4, 456–483.
Crist, E.P., 1985. A TM tasseled cap equivalent transformation for reflectance factor data. Remote Sens. Environ. 17, 301–306.
De Santis, A., Chuvieco, E., 2007. Burn severity estimation from remotely sensed data: performance of simulation versus empirical models. Remote Sens. Environ. 108, 422–435.
De Santis, A., Chuvieco, E., 2009. GeoCBI: a modified version of the Composite Burn Index for the initial assessment of the short-term burn severity from remotely sensed data. Remote Sens. Environ. 113, 554–562.
De'ath, G., Fabricius, K.E., 2000. Classification and regression trees: a powerful yet simple technique for ecological data analysis. Ecology 81, 3178–3192.
Dillon, G.K., Holden, Z.A., Morgan, P., Crimmins, M.A., Heyerdahl, E.K., Luce, C.H., 2011. Both topography and climate affected forest and woodland burn severity in two regions of the western US, 1984 to 2006. Ecosphere 2 art130.
Eidenshink, J.C., Schwind, B., Brewer, K., Zhu, Z., Quayle, B., Howard, S.M., 2007. A project for monitoring trends in burn severity. 3 (1), 3–21.
Falkowski, M.J., Evans, J.S., Martinuzzi, S., Gessler, P.E., Hudak, A.T., 2009. Characterizing forest succession with lidar data: an evaluation for the Inland Northwest, USA. Remote Sens. Environ. 113, 946–956.
Franklin, J.F., Dyrness, C.T., 1988. Natural Vegetation of Oregon and Washington. Oregon State University Press, 452 pp.
Hammill, K.A., Bradstock, R.A., 2006. Remote sensing of fire severity in the Blue Mountains: influence of vegetation type and inferring fire intensity. Int. J. Wildland Fire 15, 213–226.
Hicke, J.A., Meddens, A.J.H., Allen, C.D., Kolden, C.A., 2013. Carbon stocks of trees killed by bark beetles and wildfire in the western United States. Environmental Research Letters 8, 035032. http://dx.doi.org/10.1088/1748-9326/8/3/035032.
Hudak, A., Morgan, P., Bobbitt, M., Smith, A., Lewis, S., Lentile, L., Robichaud, P., Clark, J., McKinley, R., 2007. The relationship of multispectral satellite imagery to immediate fire effects. Fire Ecology 3 (1), 64–90.
Hudak, A.T., Crookston, N.L., Evans, J.S., Hall, D.E., Falkowski, M.J., 2008. Nearest neighbor imputation of species-level, plot-scale forest structure attributes from LiDAR data. Remote Sens. Environ. 112, 2232–2245.
Kane, V.R., Lutz, J.A., Roberts, S.L., Smith, D.F., McGaughey, R.J., Povak, N.A., Brooks, M.L., 2013. Landscape-scale effects of fire severity on mixed-conifer and red fir forest structure in Yosemite National Park. For. Ecol. Manag. 287, 17–31.
Kane, V.R., North, M.P., Lutz, J.A., Churchill, D.J., Roberts, S.L., Smith, D.F., McGaughey, R.J., Kane, J.T., Brooks, M.L., 2014. Assessing fire effects on forest spatial structure using a fusion of Landsat and airborne LiDAR data in Yosemite National Park. Remote Sens. Environ. 151, 89–101.

Kane, V.R., Cansler, C.A., Povak, N.A., Kane, J.T., McGaughey, R.J., Lutz, J.A., Churchill, D.J., North, M.P., 2015a. Mixed severity fire effects within the Rim fire: relative importance of local climate, fire weather, topography, and forest structure. For. Ecol. Manag. 358, 62–79.
Kane, V.R., Lutz, J.A., Cansler, C.A., Povak, N.A., Churchill, D.J., Smith, D.F., Kane, J.T., North, M.P., 2015b. Water balance and topography predict fire and forest structure patterns. For. Ecol. Manag. 338, 1–13.
Key, C.H., 2006. Ecological and sampling constraints on defining landscape fire severity. Fire Ecology 2 (2), 34–59.
Key, C.H., Benson, N.C., 2006. Landscape Assessment, Ground Measure of Severity of the Composition Burn Index and Remote Sensing Severity. FIREMON: Fire Effects of Inventory System. USDA Forest Service RMRS-GRT-164, Fort Collins, CO, USA.
Kolden, C.A., Rogan, J., 2013. Mapping wildfire burn severity in the Arctic tundra from downsampled MODIS data. Arct. Antarct. Alp. Res. 45, 64–76.
Kolden, C.A., Weisberg, P.J., 2007. Assessing accuracy of manually-mapped wildfire perimeters in topographically dissected areas. Fire Ecology 3 (1), 22–31.
Kolden, C.A., Lutz, J.A., Key, C.H., Kane, J.T., van Wagtendonk, J.W., 2012. Mapped versus actual burned area within wildfire perimeters: characterizing the unburned. For. Ecol. Manag. 286, 38–47.
Kolden, C.A., Abatzoglou, J.T., Lutz, J.A., Cansler, C.A., Kane, J.T., van Wagtendonk, J.W., Key, C.H., 2015a. Climate contributors to forest mosaics: ecological persistence following wildfire. Northwest Science 89, 219–238.
Kolden, C.A., Abatzoglou, J.T., Smith, A.M.S., 2015b. Limitations and utilisation of Monitoring Trends in Burn Severity products for assessing wildfire severity in the USA. Int. J. Wildland Fire 24, 1023–1028.
Lawrence, R.L., Wright, A., 2001. Rule-based classification systems using classification and regression tree (CART) analysis. Photogramm. Eng. Remote. Sens. 67, 1137–1142.
Liaw, A., Wiener, W., 2002. Classification and regression by randomForest. R News 2, 18–22http://CRAN.R-project.org/doc/Rnews.
Littell, J.S., Oneil, E.E., McKenzie, D., Hicke, J.A., Lutz, J.A., Norheim, R.A., Elsner, M.M., 2010. Forest ecosystems, disturbance, and climatic change in Washington State, USA. Clim. Chang. 102, 129–158.
Lutz, J.A., van Wagtendonk, J.W., Thode, A.E., Miller, J.D., Franklin, J.F., 2009. Climate, lightning ignitions, and fire severity in Yosemite National Park, California, USA. Int. J. Wildland Fire 18, 765–774.
Lutz, J.A., Key, C.H., Kolden, C.A., Kane, J.T., van Wagtendonk, J.W., 2011. Fire frequency, area burned, and severity: a quantitative approach to defining a normal fire year. Fire Ecology 7 (2), 51–65.
Masek, J.G., Vermote, E.F., Saleous, N.E., Wolfe, R., Hall, F.G., Huemmrich, K.F., Gao, F., Kutler, J., Lim, T.-K., 2006. A Landsat surface reflectance dataset for North America, 1990–2000. Geoscience and Remote Sensing Letters, IEEE 3, 68–72.
Miller, J.D., Thode, A.E., 2007. Quantifying burn severity in a heterogeneous landscape with a relative version of the delta Normalized Burn Ratio (dNBR). Remote Sens. Environ. 109, 66–80.
Miller, J.D., Knapp, E.E., Key, C.H., Skinner, C.N., Isbell, C.J., Creasy, R.M., Sherlock, J.W., 2009a. Calibration and validation of the relative differenced Normalized Burn Ratio (RdNBR) to three measures of fire severity in the Sierra Nevada and Klamath Mountains, California, USA. Remote Sens. Environ. 113, 645–656.
Miller, J.D., Safford, H.D., Crimmins, M., Thode, A.E., 2009b. Quantitative evidence for increasing forest fire severity in the Sierra Nevada and Southern Cascade Mountains, California and Nevada, USA. Ecosystems 12, 16–32.
Murphy, M.A., Evans, J.S., Storfer, A., 2010. Quantifying *Bufo boreas* connectivity in Yellowstone National Park with landscape genetics. Ecology 91, 252–261.
Noss, R.F., Franklin, J.F., Baker, W.L., Schoennagel, T., Moyle, P.B., 2006. Managing fire-prone forests in the western United States. Front. Ecol. Environ. 4, 481–487.
Ohmann, J.L., Spies, T.A., 1998. Regional gradient analysis and spatial pattern of woody plant communities of Oregon forests. Ecol. Monogr. 68, 151–182.
Parks, S.A., Holsinger, L.M., Miller, C., Nelson, C.R., 2015. Wildland fire as a self-regulating mechanism: the role of previous burns and weather in limiting fire progression. Ecol. Appl. 25, 1478–1492.
Peterson, G.D., 2002. Contagious disturbance, ecological memory, and the emergence of landscape pattern. Ecosystems 5, 329–338.
R Core Team, 2015. R: A Language and Environment for Statistical Computing. R Foundation for Statistical Computing.
Rehfeldt, G.E., Ferguson, D.E., Crookston, N.L., 2009. Aspen, climate, and sudden decline in western USA. For. Ecol. Manag. 258, 2353–2364.
Roberts, D.W., Cooper, S.V., 1989. Concepts and Techniques of Vegetation Mapping. General Technical Report INT-US Department of Agriculture, Forest Service, Intermountain Research Station (USA).
Roberts, S., van Wagtendonk, J., Miles, A., Kelt, D., Lutz, J.A., 2008. Modeling the effects of fire severity and spatial complexity on small mammals in Yosemite National Park, California. Fire Ecology 4 (2), 83–104.
Robinson, N.M., Leonard, S.W.J., Ritchie, E.G., Bassett, M., Chia, E.K., Buckingham, S., Gibb, H., Bennett, A.F., Clarke, M.F., 2013. Refuges for fauna in fire-prone landscapes: their ecological function and importance. J. Appl. Ecol. 50, 1321–1329.
Rollins, M.G., 2009. LANDFIRE: A nationally consistent vegetation, wildland fire, and fuel assessment. Int. J. Wildland Fire 18, 235–249.
Roy, D.R., Boschetti, L., Trigg, S.N., 2006. Remote sensing of fire severity: assessing the performance of the normalized Burn ratio. IEEE Geosci. Remote Sens. Lett. 3, 112–116.
Savage, M., Mast, J.N., Feddema, J.J., 2013. Double whammy: high-severity fire and drought in ponderosa pine forests of the Southwest. Can. J. For. Res. 43, 570–583.
Smith, A., Kolden, C.A., Tinkham, W.T., Talhelm, A.F., Marshall, J.D., Hudak, A.T., Boschetti, L., Falkowski, M.J., Greenberg, J.A., Anderson, J.W., 2014. Remote sensing the vulnerability of vegetation in natural terrestrial ecosystems. Remote Sensing of Environment 153, 322–337.
Smith, A.M., Kolden, C.A., Paveglio, T.B., Cochrane, M.A., Bowman, D.M., Moritz, M.A., Kliskey, A.D., Alessa, L., Hudak, A.T., Hoffman, C.M., Lutz, J.A., Queen, L.P., Goetz, S.J., Higuera, P.E., Boschetti, L., Flannigan, M., Yedinak, K.M., W.A., C., Strand, E.K., van Wagtendonk, J.W., Anderson, J.W., Stocks, B.J., Abatzoglou, J.T., 2016. The science of firescapes: achieving fire-resilient communities. Bioscience 66, 130–146.
Sparks, A.M., Boschetti, L., Smith, A.M., Tinkham, W.T., Lannom, K.O., Newingham, B.A., 2015. An accuracy assessment of the MTBS burned area product for shrub-steppe fires in the northern Great Basin, United States. Int. J. Wildland Fire 24, 70–78.
Speybroeck, N., 2012. Classification and regression trees. International Journal of Public Health 57, 243–246.
Spracklen, D.V., Mickley, L.J., Logan, J.A., Hudman, R.C., Yevich, R., Flannigan, M.D., Westerling, A.L., 2009. Impacts of climate change from 2000 to 2050 on wildfire activity and carbonaceous aerosol concentrations in the western United States. Journal of Geophysical Research: Atmospheres 114.
Stage, A.R., 1976. Notes: an expression for the effect of aspect, slope, and habitat type on tree growth. For. Sci. 22, 457–460.
Swanson, M.E., Franklin, J.F., Beschta, R.L., Crisafulli, C.M., DellaSala, D.A., Hutto, R.L., Lindenmayer, D.B., Swanson, F.J., 2010. The forgotten stage of forest succession: early-successional ecosystems on forest sites. Front. Ecol. Environ. 9, 117–125.
Swengel, A.B., Swengel, S.R., 2007. Benefit of permanent non-fire refugia for Lepidoptera conservation in fire-managed sites. J. Insect Conserv. 11, 263–279.
Therneau, T., Atkinson, B., Ripley, B., 2015. rpart: recursive partitioning and regression trees. Version 4, 1–10https://CRAN.R-project.org/package=rpart.
Thompson, J.R., Spies, T.A., Ganio, L.M., 2007. Reburn severity in managed and unmanaged vegetation in a large wildfire. Proceedings of the National Academy of Sciences of the United States of America *104*, 10743–10748.
Trigg, S., Flasse, S., 2001. An evaluation of different bi-spectral spaces for discriminating burned shrub-savannah. Int. J. Remote Sens. 22, 2641–2647.
Tucker, C.J., 1979. Red and photographic infrared linear combinations for monitoring vegetation. Remote Sens. Environ. 8, 127–150.
van Wagtendonk, J.W., Lutz, J.A., 2007. Fire regime attributes of wildland fires in Yosemite National Park, USA. Fire Ecology 3 (2), 34–52.
van Wagtendonk, J.W., Root, R.R., Key, C.H., 2004. Comparison of AVIRIS and Landsat ETM+ detection capabilities for burn severity. Remote Sens. Environ. 92, 397–408.
Vogelmann, J.E., 1990. Comparison between 2 vegetation indexes for measuring different types of forest damage in the north-eastern United States. Int. J. Remote Sens. 11, 2281–2297.
Vogelmann, J.E., Rock, B.N., 1988. Assessing forest damage in high-elevation coniferous forests in Vermont and New-Hampshire using Thematic Mapper data. mote Sens. Environ. 24, 227–246.
White, J.D., Ryan, K.C., Key, C.C., Running, S.W., 1996. Remote sensing of forest fire severity and vegetation recovery. Int. J. Wildland Fire 6, 125–136.
Wilson, E.H., Sader, S.A., 2002. Detection of forest harvest type using multiple dates of Landsat TM imagery. Remote Sens. Environ. 80, 385–396.
Zhu, Z., Woodcock, C.E., 2012. Object-based cloud and cloud shadow detection in Landsat imagery. Remote Sens. Environ. 118, 83–94.